ADVANCED FUNCTIONAL MATERIALS
www.afm-journal.de

Multiplex SERS Detection of Metabolic Alterations in Tumor Extracellular Media

*Javier Plou, Isabel García, Mathias Charconnet, Ianire Astobiza, Clara García-Astrain, Cristiano Matricardi, Agustín Mihi, Arkaitz Carracedo, and Luis M. Liz-Marzán**

The composition and intercellular interactions of tumor cells in the tissues dictate the biochemical and metabolic properties of the tumor microenvironment. The metabolic rewiring has a profound impact on the properties of the microenvironment, to an extent that monitoring such perturbations could harbor diagnostic and therapeutic relevance. A growing interest in these phenomena has inspired the development of novel technologies with sufficient sensitivity and resolution to monitor metabolic alterations in the tumor microenvironment. In this context, surface-enhanced Raman scattering (SERS) can be used for the label-free detection and imaging of diverse molecules of interest among extracellular components. Herein, the application of nanostructured plasmonic substrates comprising Au nanoparticles, self-assembled as ordered superlattices, to the precise SERS detection of selected tumor metabolites, is presented. The potential of this technology is first demonstrated through the analysis of kynurenine, a secreted immunomodulatory derivative of the tumor metabolism and the related molecules tryptophan and purine derivatives. SERS facilitates the unambiguous identification of trace metabolites and allows the multiplex detection of their characteristic fingerprints under different conditions. Finally, the effective plasmonic SERS substrate is combined with a hydrogel-based three-dimensional cancer model, which recreates the tumor microenvironment, for the real-time imaging of metabolite alterations and cytotoxic effects on tumor cells.

1. Introduction

Cancer cells and the stroma create dynamic pseudo-organs that contain a unique niche with distinct biochemical and physiological properties. During the progression of the disease, tumor and stromal cells exhibit bidirectional alterations in their interaction modes and patterns of co-evolution.[1] As a result, the mutations and signaling alterations in tumor cells modify the composition of the microenvironment, whereas changes in the microenvironment can also influence the fitness of cancer cells. The reprogramming of cancer metabolism represents a biochemical process that sustains cancer growth and proliferation, while also exerting a profound influence in the tumor microenvironment.[2–4] Several lines of evidence support the notion that symbiotic and competitive mechanisms exist, stemming from distinct metabolite-based communication, which support tumor growth and hinder antitumor immunity. Consequently, the assessment of tumor-secreted

J. Plou, Dr. I. García, M. Charconnet, C. García-Astrain, Prof. L. M. Liz-Marzán
CIC biomaGUNE
Basque Research and Technology Alliance (BRTA)
Paseo de Miramón 182, 20014 Donostia-San Sebastián, Spain
E-mail: llizmarzan@cicbiomagune.es

J. Plou, Dr. I. García, Prof. L. M. Liz-Marzán
Biomedical Research Networking Center in Bioengineering Biomaterials, and Nanomedicine, CIBER-BBN
20014 Donostia-San Sebastián, Spain

J. Plou, Dr. I. Astobiza, Prof. A. Carracedo
CIC bioGUNE
Basque Research and Technology Alliance (BRTA)
48160 Derio, Spain

M. Charconnet
CIC nanoGUNE Consolider
Basque Research and Technology Alliance (BRTA)
20018 Donostia-San Sebastián, Spain

Dr. I. Astobiza, Prof. A. Carracedo
Biomedical Research Networking Center in Oncology
CIBERONC
48160 Derio, Spain

C. Matricardi, Dr. A. Mihi
Instituto de Ciencia de Materiales de Barcelona (ICMAB-CSIC)
08193 Bellaterra, Spain

Prof. A. Carracedo
Biochemistry and Molecular Biology Department
University of the Basque Country (UPV/EHU)
48940 Bilbao, Spain

Prof. A. Carracedo, Prof. L. M. Liz-Marzán
Ikerbasque
Basque Foundation for Science
48013 Bilbao, Spain

The ORCID identification number(s) for the author(s) of this article can be found under https://doi.org/10.1002/adfm.201910335.

DOI: 10.1002/adfm.201910335

metabolites becomes instrumental for monitoring the response of tumors upon therapeutic challenges, the stratification of cancer patients, and the identification of novel therapeutic strategies. In this regard, imaging and fast detection of metabolites can play a critical role to accomplish these aims.[5–7]

Traditionally, extracellular metabolic studies have been carried out by means of colorimetric techniques, which involve the addition of chemical groups that specifically react with the molecule of interest. Such methods are rapid and convenient but have also significant drawbacks, as they are invasive and do not allow the long-term simultaneous detection of multiple analytes.[8] More recently, liquid chromatography (LC)–coupled mass spectrometry (MS) has been the technique of choice for the majority of high- and low-throughput metabolic analyses, due to its robustness and multiple detection capability. However, LC-MS involves time-consuming, expensive, and destructive procedures.[9] Nuclear magnetic resonance (NMR) is the other common analytical tool in metabolomics research.[10] NMR allows quantifying most components in biological fluids with no need for elaborate sample preparation; however, the sensitivity of NMR spectroscopy remains a weak point, as compared, e.g., to LC-MS.[11] Hence, the development of alternative label-free methods to rapidly detect multiple tumor-secreted metabolites in extracellular media is required toward understanding metabolic interactions in the tumor niche.[12]

Surface-enhanced Raman scattering (SERS) spectroscopy, an optical ultrasensitive analytical method that can be applied noninvasively for label-free detection and imaging of a wide range of analytes, stands as a promising technique that fulfills several of the above-mentioned requirements.[13] SERS allows the identification of vibrational fingerprints of probe molecules in contact with a plasmonic nanostructure, and its sensitivity can go as far as the single-molecule level.[14] Therefore, SERS has emerged as a promising method for the detection and characterization of biological molecules in solution and within cells for cancer diagnosis.[15,16] On the one hand, on account of the complexity related to the interpretation of spectra obtained in biological media, much work has focused on comparing spectra of samples from healthy and cancer patients.[17–20] On the other hand, efforts have been made to computationally decipher the contributions of a number of analytes to the final SERS spectra.[21,22]

We report a SERS-based strategy to monitor the extracellular accumulation of metabolites relevant to tumor biology, applying a recently developed nanostructured plasmonic substrate comprising a superlattice of Au nanoparticles, as the source of enhancement for the Raman signal from the analytes (**Scheme 1**). Our results support the potential of this technology for nondestructive and sensitive detection of metabolites in the extracellular compartment, which we demonstrate through the detection of immunomodulatory kynurenine (Kyn) and tryptophan (Trp), and the setup of a cytotoxicity assay based on the detection of purine derivatives. We then implemented this SERS-based detection system to image the accumulation of purine derivatives in cancer-on-a-chip models, thereby achieving spatiotemporal monitoring of cell death upon induction of cellular stress. The quality of the recorded SERS spectra reinforced the efficiency and versatility of the method for the label-free molecular detection of small metabolites in the extracellular medium, and its potential contribution to understanding the fluctuations of such molecules within the tumor microenvironment.

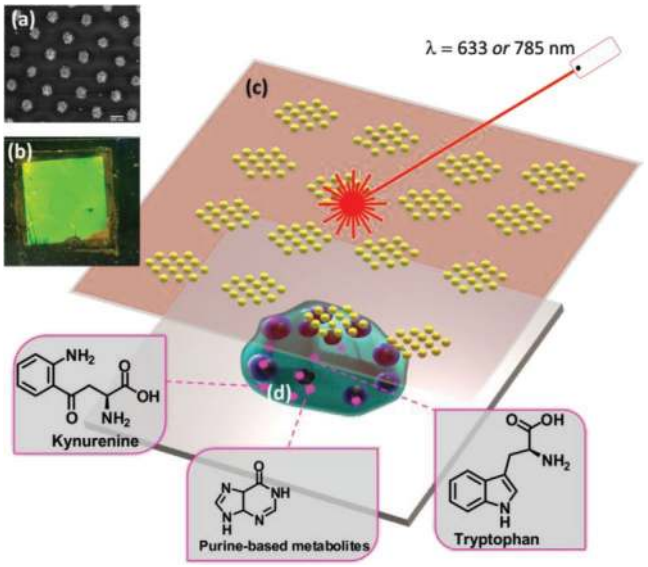

Scheme 1. Schematic illustration of the SERS-based system to detect the accumulation of metabolites in the extracellular tumor milieu. a–c) Nanostructured plasmonic substrate comprising a superlattice of Au nanoparticles. d) Chemical structures of the different tumor associated metabolites accumulated in the tumoral extracellular microenvironment.

2. Results and Discussions

2.1. Plasmonic Substrates for SERS Detection of Kynurenine and Tryptophan

We initially studied the application of SERS to identify the presence of selected metabolites, commonly secreted by cancer cells and relevant to tumor biology, including tryptophan, kynurenine, and purine derivatives.[23,24] We tested two types of plasmonic substrates, which were previously optimized for the detection of bacterial Quorum sensing signaling molecules.[25,26] Although both strategies involve the deposition of 30 nm spherical Au nanoparticles (AuNPs) on glass substrates, the different methodologies (see "Experimental Section" for detailed descriptions) result in radically different distributions of AuNPs on the substrate.[25,26] On the one hand, the standard polyelectrolyte layer-by-layer (LbL) assembly methodology was used to produce homogeneous (disordered) multilayers of AuNPs on a glass cover slip (a schematic description of the fabrication is shown in Figure S1a in the Supporting Information). On the other hand, a recently developed template-assisted self-assembly process resulted in the formation of hierarchical nanostructured substrates, comprising square arrays of hexagonally packed AuNP clusters (see **Figure 1**a), so-called plasmonic superlattices (a graphical representation of the fabrication procedure is shown in Figure S1b in the Supporting Information). The different AuNP organizations resulted in significant differences in the extinction spectra of the substrates. Comparison of the spectra (normalized to the amount of gold) for both

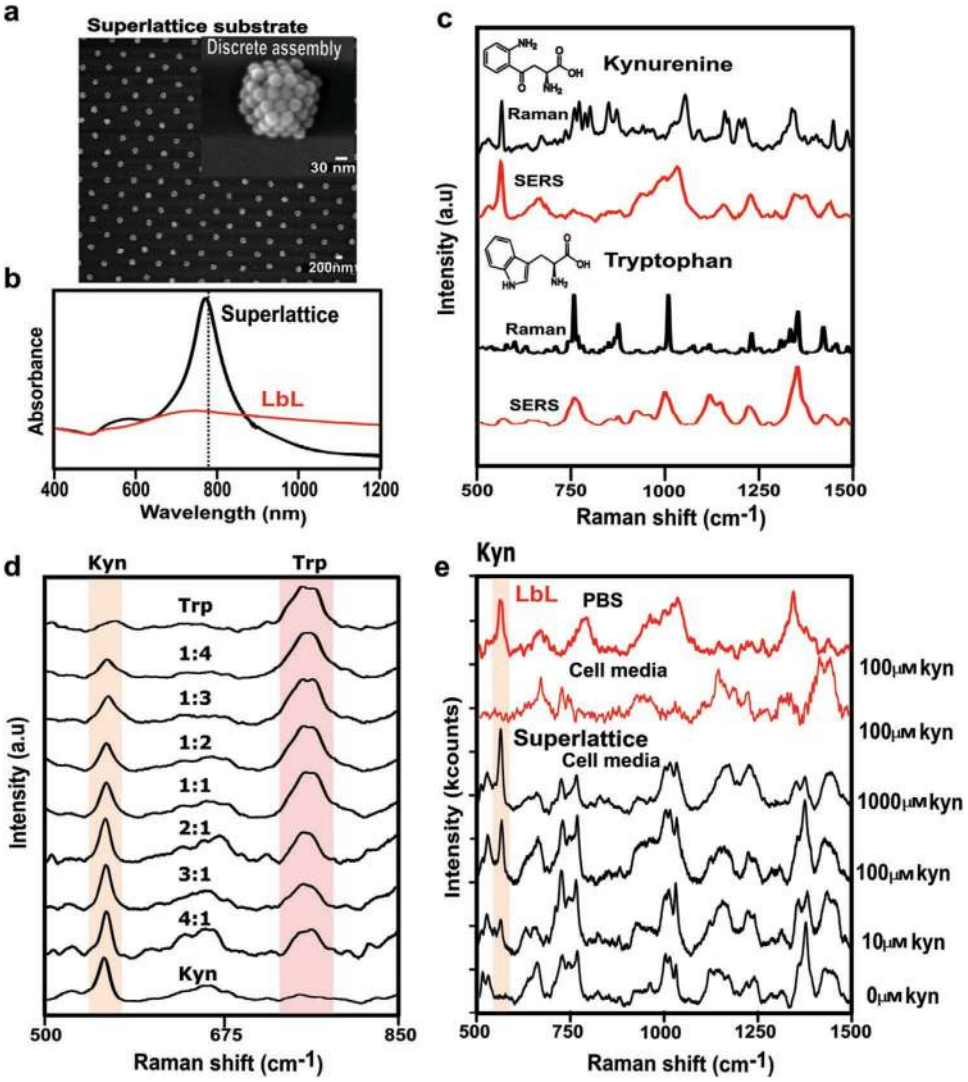

Figure 1. a) Representative scanning electron microscopy (SEM) image of the organized discrete assemblies of Au nanospheres in the superlattice substrate. The inset shows the structure of a representative NP assembly. b) Vis–NIR spectra, normalized to 400 nm, for both LbL and superlattice plasmonic substrates; the vertical line indicates the excitation wavelength used for SERS measurements (785 nm). c) Comparison of Raman and SERS spectra for kynurenine (Kyn) and tryptophan (Trp), measured in the solid state (black) and in 100×10^{-6} M aqueous solution deposited on a superlattice substrate (red). All measurements were performed with a 50× objective, 10 s acquisition time, and a maximum power of the 785 nm laser of 295.13 kW cm^{-2}. d) SERS spectra of kynurenine–tryptophan mixtures with different ratios; the kynurenine characteristic peak (560 cm^{-1}) is highlighted with an orange bar and the tryptophan peak (760 cm^{-1}) with a pink bar. e) SERS spectra from different plasmonic substrates, in PBS and cell media. The presence of cell media masks the signal of the kynurenine peak at 560 cm^{-1} (orange label) and prevents its quantification in LbL substrates (red).

substrates revealed that the plasmonic superlattices support a sharp resonance around 760 nm, which closely matched the 785 nm SERS excitation laser wavelength, whereas LbL films displayed a much broader extinction band, while retaining a maximum within the same wavelength range (Figure 1b). This significant difference is due to Rayleigh anomalies occurring in periodic plasmonic structures, as previously reported.[27] This physical phenomenon occurs when in-plane diffracted waves interact with the gold nanoparticle clusters, resulting in an enhancement of the plasmon resonance around the wavelength of the Rayleigh anomaly, which also results in an additional increase of the electric near-field within each AuNP cluster (Figure S2, Supporting Information). This event, also known as lattice plasmon resonance, can be modulated into a desired wavelength range, by varying the lattice period of the plasmonic substrate. We selected a lattice parameter (L) of 500 nm to obtain a lattice plasmon resonance around 760 nm, i.e., closely matching the excitation laser wavelength of 785 nm for SERS experiments (Figure S3, Supporting Information).

Shown in Figure 1c are Raman and SERS spectra of commercial Kyn and Trp, recorded both in the solid state and in solution. For SERS measurements, 100 µL of a 100×10^{-6} M analyte solution was deposited on the corresponding nanostructured plasmonic substrate and subsequently illuminated with the 785 nm laser. The obtained results show that the Kyn SERS spectrum is dominated by a narrow peak at 560 cm^{-1}, corresponding to the aminophenyl group.[28] The SERS spectrum of Trp was characterized by broader peaks, including

one localized around 760 cm^{-1}, which corresponds to the indole moiety.[29] SERS spectra of commercial Kyn and Trp at different concentrations were then collected and compared to the SERS spectrum of phosphate-buffered saline (PBS) on the same plasmonic support, used as a blank. For both analytes, 1×10^{-6} M was the lowest concentration that could be safely distinguished from the blank. This limit of detection is sufficient for the detection of both metabolites in the extracellular space ($\approx$ (10–100) $\times 10^{-6}$ M).[30] In addition, we observed a correlation between metabolite concentration and SERS intensity within this concentration range (see Figure S4a in the Supporting Information).

The concentrations of both selected metabolites (Kyn and Trp) in extracellular media are regulated by indoleamine 2,3-dioxygenase 1 (IDO-1) enzyme, which is overexpressed in many tumor cell types. More specifically, IDO-1 utilizes Trp to generate Kyn, thereby impoverishing the extracellular milieu in Trp and enriching it in Kyn (Figure S4c, Supporting Information). This metabolic reaction has recently attracted much attention as a consequence of the association of high Kyn/Trp ratios in plasma from cancer individuals with poor patient prognosis.[31,32] In this context, we hypothesized that the implementation of a SERS detection scheme would provide an efficient methodology to monitor Kyn/Trp ratio in the extracellular environment, and in turn for the extrapolation of IDO-1 expression. For the initial determination of the Kyn/Trp ratio, the metabolites were co-incubated on superlattice substrates at varying relative concentrations. The characteristic SERS spectral features allow simultaneous determination of both metabolites, using the peak at 560 cm^{-1} for Kyn and that at 760 cm^{-1} for Trp, which are sufficiently well differentiated in spite of being a closely related pair of analytes. As shown in Figure 1d, the relative contribution of the selected fingerprint peaks gradually changed for different Kyn/Trp ratios. We can therefore estimate the Kyn/Trp ratio from the corresponding ratio between the SERS intensities of these main peaks. Our results confirmed that semiquantitative monitoring of both analytes could be achieved for the selected tryptophan–kynurenine combinations (Figure S4d, Supporting Information). Similar results for Kyn and Trp detection could be achieved using LbL multilayer substrates (Figure S5, Supporting Information).

It should be noted that the aforementioned experiments were performed in simple metabolite solutions, far from the complexity found in real biofluids, where Kyn and Trp are a minor fraction, and the likelihood of interference using SERS would significantly increase. In fact, detection of specific metabolites within complex environments is considered as one of the major challenges to be addressed by optical-based detection systems.[12,33] Although both plasmonic substrates were sufficiently efficient to identify Kyn in PBS, when we incubated varying concentrations of Kyn in cell media, discrepancies were observed between the spectra obtained using both substrates (see Figure S6a,b in the Supporting Information). As shown in Figure 1e, only the superlattice substrate was reliable toward the detection of kynurenine in complex media, whereas no significant bands at 560 cm^{-1} could be identified using LbL substrates. This result is in agreement with the improved plasmonic performance, based on the excitation of lattice plasmon modes when exciting the superlattice at 785 nm. Importantly, when we employed plasmonic superlattice structures, the detection of kynurenine was confirmed at 10×10^{-6} M in cell media.

2.2. Analysis of the Metabolic Alterations Induced by IDO-1 Expressing Cells

We therefore selected the nanostructured plasmonic superlattice substrates to study extracellular metabolic alterations, as well as the activity of IDO-1 in tumor cells under different conditions. For this purpose, HeLa cells were challenged with interferon-gamma (IFN-ϒ) as a suitable model to activate IDO-1 expression.[30,34] HeLa cells treated with IFN-ϒ (100 ng mL^{-1}) consistently induced IDO-1 expression (Figure S7, Supporting Information). Cells challenged with IFN-ϒ were rinsed, and fresh media were supplemented with varying Trp concentration, in order to monitor its conversion to Kyn. Of note, media were also supplemented with 10×10^{-6} M of hemin, a co-factor of IDO-1 enzyme, which is necessary for the tryptophan catalytic conversion.[35,36] High performance liquid chromatography coupled to mass spectrometry (HPLC-MS)-based metabolic measurements of Trp and Kyn confirmed the IFN-ϒ-elicited conversion of Trp to Kyn, due to induced IDO-1 expression (Figures S8–S11, Supporting Information). As shown in **Figure 2**a, consistent differences were observed between spectra recorded from various cell supernatants. IFN-ϒ treatment of HeLa cells resulted in the detection of a SERS signal indicating the presence of Kyn (560 cm^{-1}) (see Figure S12 in the Supporting Information), whereas no signal was identified in control experiments. In addition, the absence of supplemented Trp in media prevented the accumulation of Kyn, in line with the lack of IDO-1 substrate. Subsequently, we calculated the Kyn/Trp ratio as described above, resulting in data for the ratio between both metabolites (Figure 2b). Increasing Trp was consistently accompanied by lower Kyn SERS signal. Additionally, SERS measurements allowed us to study time-dependent changes in cell media, under the same conditions of tryptophan (100×10^{-6} M) and IFN-ϒ treatment (Figure 2c).

As a complementary approach to promote the production of Kyn, we chose to expose HeLa cells to increasing doses of an IDO-1 co-activator analog, hemin, as a commercial analog of the heme group, a non-polypeptide unit required for the biological function of IDO-1. As shown in Figure 2d, hemin supplement was required for Kyn production, in agreement with its impact on the activation of IDO-1. We observed that hemin addition affected the recorded SERS profile in a dose-dependent manner, beyond the sharp signal at 560 cm^{-1}. Figure 2e illustrates that high hemin concentrations (100×10^{-6} M) resulted in the detection of an intense SERS band at 725 cm^{-1}, commonly assigned to purine derivative metabolites.[37] We also observed an increase in cell death at high hemin concentration, which suggested a cytotoxic effect of this co-factor (Figure S13, Supporting Information).[38] This cellular process drove us to speculate that both events, cell death and the release of purine derivatives, were correlated and could be investigated by SERS.

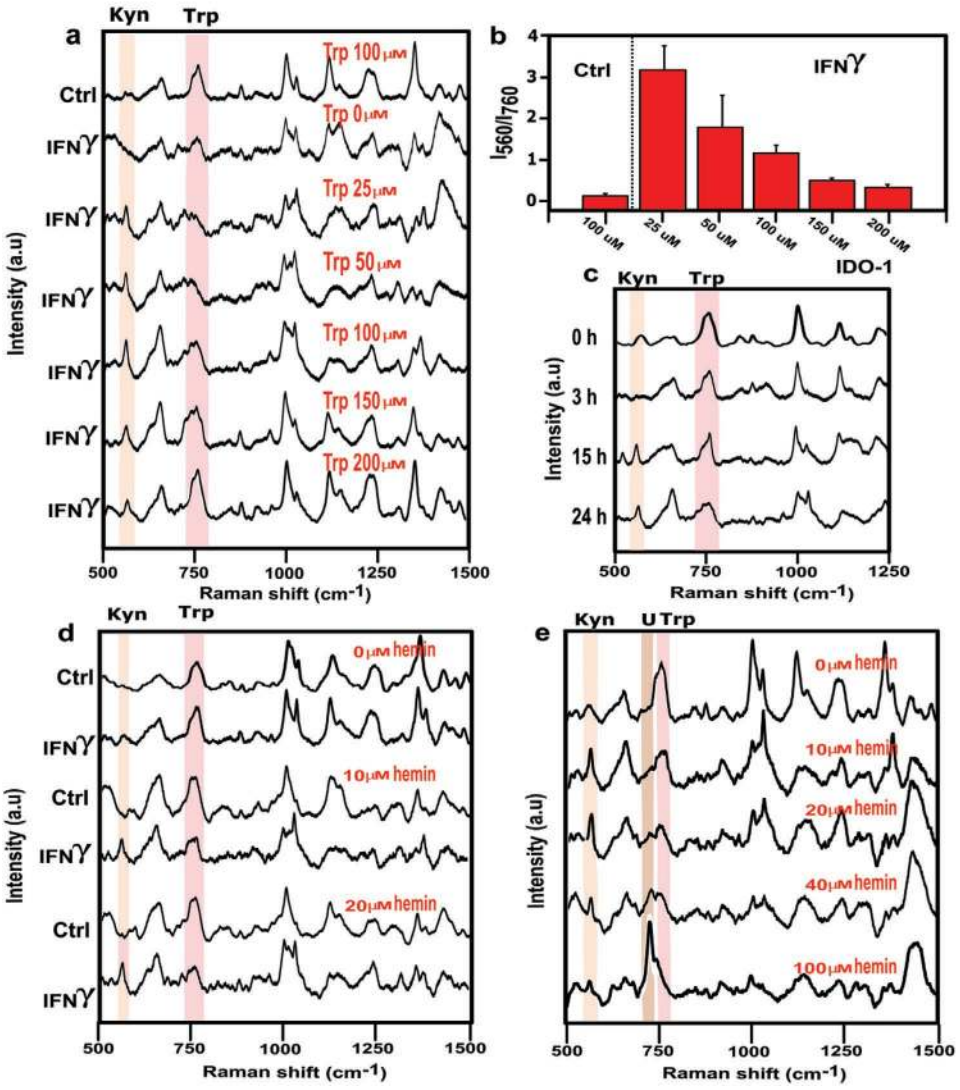

Figure 2. a) SERS spectra of cell supernatants after 24 h. Cells were harvested, varying the addition of IFN-ϒ, which induces the expression of IDO-1 enzyme, and the initial tryptophan concentration. The orange bar tracks the kynurenine peak while the tryptophan signal is indicated by a pink bar. The spectra are the average spectrum of 25 measurements from a representative sample. b) Ratio between kynurenine (560 cm^{-1}) and tryptophan (760 cm^{-1}) in control and after 3 days of IFN-ϒ conditions (100 ng mL^{-1}) and Trp supplementation from 25×10^{-6} to 200×10^{-6} M, as calculated from SERS data. The error bars show the standard deviation of three independent cell assays. c) SERS spectra of cell supernatants extracted at different times. Cells were previously activated with IFN-ϒ and incubated with 100×10^{-6} M of Trp. d) SERS spectra of cell supernatant obtained from cells which were incubated with 100×10^{-6} M of Trp and varying addition of IFN-ϒ and hemin concentrations (0, 10×10^{-6}, and 20×10^{-6} M) e) SERS spectra of cell supernatant of IFN-ϒ activated cells and incubated with 100×10^{-6} M of Trp and varying concentrations of hemin (0, 10×10^{-6}, 20×10^{-6}, 40×10^{-6}, and 100×10^{-6} M). The brown bar tracks the presence of the peak at 725 cm^{-1}, named U as an undefined event. SERS measurements were performed with a 50× objective and 10 s of acquisition time, and the maximum power of the 785 nm laser was 295.13 kW cm^{-2}.

2.3. Detection of Extracellular Hypoxanthine Accumulation in Cell Death Events

Recent studies put the focus on the crucial role of purine derivative metabolites within the extracellular environment and how anticancer therapies can promote the accumulation of these molecules in the extracellular milieu of tumors.[39–42] From the unexpected results obtained in the above-described experiments, we envisioned the biological value of monitoring variations of purine derivatives by SERS, to sense changes in tumor environment. Initially, we measured a number of representative purine derivative metabolites, such as ATP, adenine, adenosine, inosine, and hypoxanthine (HX). The recorded SERS spectra provided a moderate distinction between adenine and hypoxanthine as shown in **Figure 3**a. In particular, a mild shift was observed in the main peak, from 735 cm^{-1} in adenine-related molecules (black) to 725 cm^{-1} in hypoxanthine derivatives (red). This spectral modification can be attributed to chemical variations, more specifically, the deamination process, between adenine and hypoxanthine nitrogenous bases.[43] The molecular structure of both bases (see the inset in Figure 3a) reflects that adenine contains an extra amino group in the purine ring, compared to hypoxanthine.

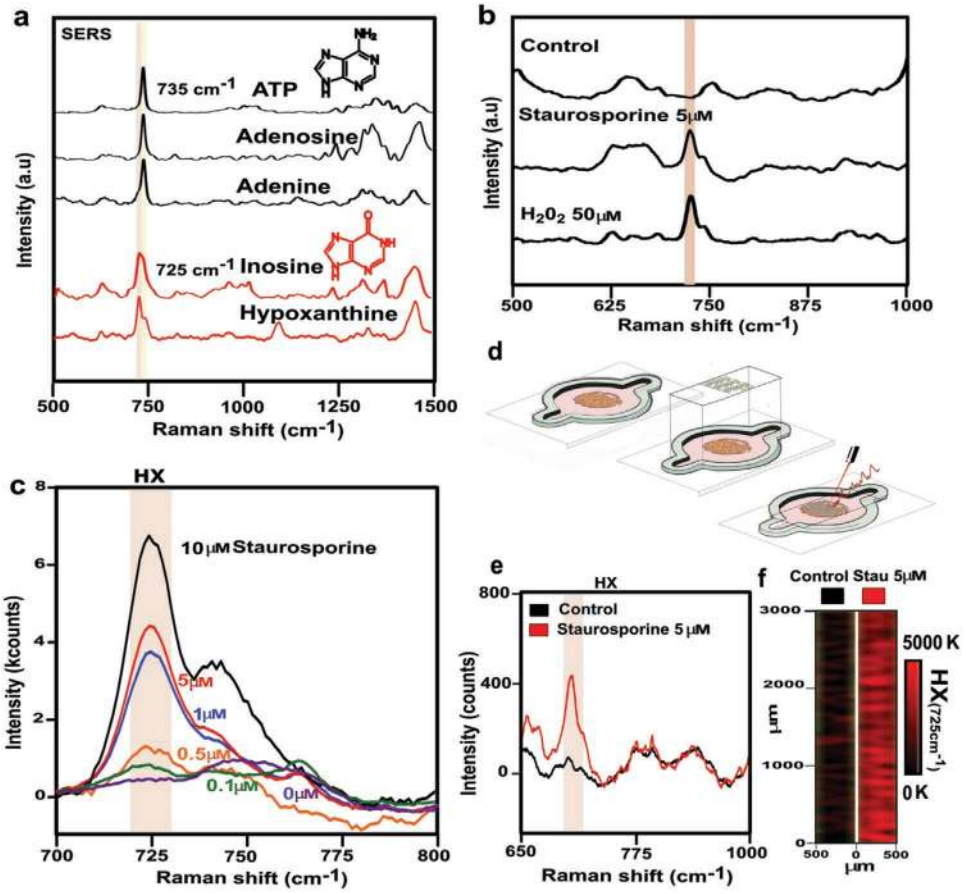

Figure 3. a) SERS spectra of adenine and hypoxanthine derivate metabolites; brown and yellow bars identify the characteristic peak of hypoxanthine (725 cm^{-1}) and adenine (735 cm^{-1}), respectively. SERS measurements were performed with a 50× objective, and the maximum power of the 785 nm laser was 295.13 kW cm^{-2} and 10 s of acquisition time. b) SERS spectra of cell supernatants extracted after 24 h of cell culture, under different stress conditions. The contribution to the averaged spectra of adenine- and hypoxanthine-related molecules is highlighted by brown and yellow bars, respectively. The spectra are the average of 25 measurements on a representative sample. c) SERS spectra of cell supernatants after 24 h of cell incubation with different staurosporine concentrations. The spectra are the average of 25 measurements on a representative sample. d) Schematic view of the methodology used to combine a 3D cell culture inside a silicon chamber with SERS measurements. e) Average of SERS spectra recorded under different staurosporine concentrations. f) SERS mapping (725 cm^{-1}) acquired with an excitation laser wavelength of 785 nm,10× objective, and a laser power of 115.95 kW cm^{-2}, for 5 s.

To demonstrate that SERS can be effectively employed to detect the release of these purine bases in the extracellular milieu, we exposed HeLa cells to diverse stress conditions, such as high concentrations of hydrogen peroxide and staurosporine, which are well-defined inducers of apoptosis.[44] We measured the SERS spectra from cell supernatants after 24 h under the selected conditions. We found that, indeed, SERS signals corresponding to the accumulation of purine derivatives were markedly altered under stress conditions, in an analogous manner as previously observed in hemin addition experiments (Figure 3b). We finally tested whether drug concentration would correlate with the intensity of the peak at 725 cm^{-1}, which can be partly attributed to HX (Figure S14, Supporting Information). From the results displayed in Figure 3c, we observed a rising trend, which reached a maximum at 10×10^{-6} M of staurosporine, when a high percentage of the cells were dead (Figure S15a, Supporting Information). Interestingly, the percentage of cell death obtained from cell viability assays showed a good correlation with the trend observed from the SERS intensity of the peak at 725 cm^{-1} (Figure S15b,c, Supporting Information). This similarity, together with the results obtained by HPLC-MS analysis (Figures S16 and S17, Supporting Information), strengthens the idea that both events are connected.

In view of the sensitivity of the results achieved through SERS detection of purine derivative metabolites, we went a step further toward the application of SERS for in situ sensing of different analytes in hydrogel-based cancer models. For this purpose, we designed a configurable cancer-on-a-chip system which mimicked a more physiologically relevant three-dimensional (3D) structure of collagen,[45,46] and then explored the combination of this platform with plasmonic substrates (Figure 3d). We initially cultured a collagen bioink laden with HeLa cells inside printed silicone chambers, filled with cell media, up to the selected time to make SERS measurements, then, the chamber was stacked with the plasmonic substrate and illuminated with the 785 nm laser (Figure S18, Supporting Information). We found that SERS signals corresponding to the accumulation of HX in the extracellular media could still be detected under stress

conditions, namely 5×10^{-6} M staurosporine (Figure 3e). On the other hand, SERS mapping of control cells (no staurosporine addition) did not reveal any significant signal of HX production. Interestingly, as shown in Figure 3d, plasmonic monitoring of HX molecules could be performed, by following the intensity of the peak at 725 cm^{-1} over large (millimeter-scale) regions of the extracellular environment, without disrupting the system. The uniformity of HX levels in the maps recorded under stress conditions indicates a suitable diffusion of HX from the hydrogel-based cancer model to the plasmonic substrate.

2.4. Imaging of Hemin Cytotoxic Effect in 3D Cell Culture

We finally exploited the cancer-on-a-chip system for the in situ sensing of hemin concentrations and its cytotoxic effect by SERS. Hemin molecules exhibit a broad absorption band in the visible, which drops at 700 nm, so that illumination of an aqueous solution of commercial hemin with a 633 nm laser leads to resonant Raman conditions. Therefore, surface-enhanced resonance Raman scattering (SERRS) rather than SERS spectra of hemin were recorded (Figure S19, Supporting Information). Our choice of plasmonic superlattices as SERS substrates offers the possibility of varying the lattice parameter to obtain a lattice plasmon mode in resonance with the 633 nm laser (**Figure 4**a).[27] The results plotted in Figure 4b illustrate the achieved improvement in hemin detection when the lattice plasmon wavelength of the substrate matched the 633 nm excitation laser, through the SERRS pyrrole ring vibration signal of hemin. As a consequence, we reconfigured the system over the course of the experimental protocol (watch Videos S1 and S2 in the Supporting Information), alternating plasmonic substrates

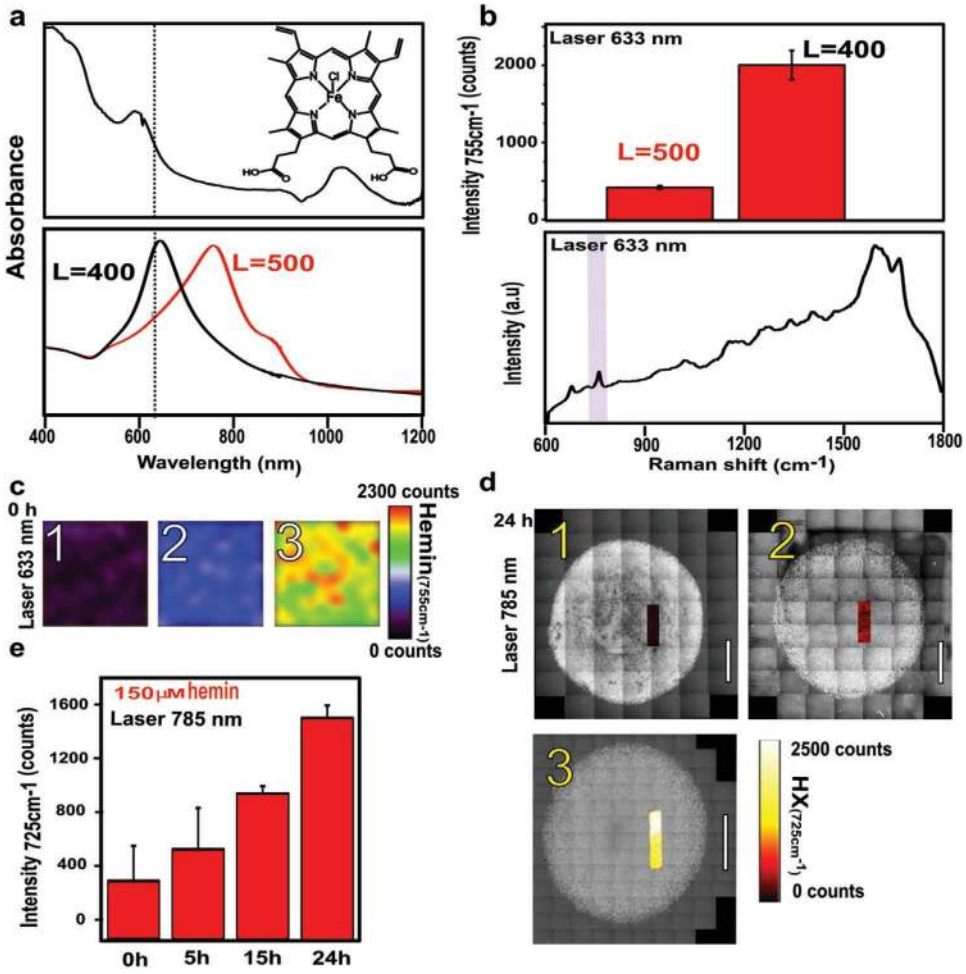

Figure 4. a) Normalized vis–NIR spectrum and chemical structure of hemin (upper panel) and normalized vis–NIR spectra of plasmonic superlattices with different lattice parameters, as labeled. The dotted vertical line indicates the excitation wavelength (633 nm) used for the SERRS measurements of hemin. b) SERRS spectrum of hemin and the corresponding intensities of the peak at 755 cm^{-1} (purple bar), as a function of the lattice parameter. The measurements were recorded with a 50× objective, a maximum laser (633 nm) power of 51.87 kW cm^{-2}, and an acquisition time of 10 s. The spectrum is the average of 25 measurements. c) SERRS mapping (755 cm^{-1}) after addition of different hemin concentrations: 1 (0 M), 2 (75×10^{-6} M), and 3 (150×10^{-6} M), acquired under the same conditions. d) Optical image of the hydrogel-based cancer model captured with a cell observer microscope and superimposed with the corresponding HX SERS mapping (725 cm^{-1}) of a selected area. Yellow numbers indicate different initial hemin concentrations: 1 (0 M), 2 (75×10^{-6} M), and 3 (150×10^{-6} M), scale bar: 2 mm. e) Relative SERRS intensities, 725 cm^{-1}, recorded at 0, 5, 15, and 24 h of incubation with the highest hemin concentration (150×10^{-6} M); error bars refer to standard deviation of three different measurements. All measurements were acquired with an excitation laser wavelength of 785 nm, 10× objective, and a laser power of 115.95 kW cm^{-2} for 10 s.

with different lattice parameters (L = 400 or 500 nm), so as to efficiently match the different laser wavelengths (633 and 785 nm), thereby being able to detect both hemin and HX.

We first challenged the 3D cell cultures with two different hemin concentrations (75×10^{-6} and 100×10^{-6} M) and monitored them in the cancer-on-a-chip platform by SERRS (633 nm laser; L = 400 nm), as shown in Figure 4c and in the SERS/SERRS spectra shown in Figure S20 (Supporting Information). After 24 h, we reconfigured the system by replacing the plasmonic substrates (L = 500 nm) and illuminated with the 785 nm laser. The results shown in Figure 4d illustrate the effect of hemin on the extracellular HX concentration, again confirming that higher hemin concentration results in higher release of HX (Figure S21a, Supporting Information). Thus, we evaluated the effect of the highest hemin concentration over time. Notably, the SERS fingerprint of HX was clearly identified as early as 5 h after initiating the treatment, and the signal intensity increased over time, as shown by the SERS spectra recorded at 15 and 24 h (Figure 4e). This indicates that hemin can have an early cytotoxic effect on cancer cells, by altering the extracellular milieu (Figure S21b, Supporting Information).

3. Conclusions

The present study demonstrates the application of surface-enhanced Raman scattering to the detection of extracellular tumor metabolites under diverse cell culture conditions. IDO-1 activity in tumor cells was monitored by SERS, measuring simultaneously extracellular changes in both the substrate and the product of the enzymatic activity (Trp and Kyn, respectively). By using highly efficient nanostructured plasmonic substrates we were able to estimate by SERS the Kyn/Trp ratio, which is well known to correlate with bad prognosis in cancer patients. On the other hand, we observed that the co-factor of IDO-1 enzyme, hemin, affects the SERS profile in a dose-dependent manner, and this SERS signal was further associated with the induction of cell death at toxic concentrations of hemin. Additionally, we observed that the levels of purine derivative metabolites were directly related to cell death induction, working as a suitable biomarker of cell death. Finally, the reported approach provided an additional tool for the spatiotemporal analysis of metabolite alterations and their response under different conditions. We demonstrated that these label-free studies can be extended to in situ imaging of metabolite exchange in tumor microenvironments, without disturbing the samples under investigation. This sensitive and cost-effective plasmonic substrate was effectively combined with 3D cell culture models, which more closely recreate the biochemical and biophysical factors in the tumor microenvironment, toward a real-time imaging of heterogeneous metabolic alterations and cytotoxic effects on tumor cells, which will have significance in diagnosis and therapy. Additionally, the development of standardized protocols and data-processing programs for multiple metabolite quantification in complex environments appears as a crucial advancement to extend these SERS-based metabolomics studies to a greater variety of metabolites from different diseases in vivo.

4. Experimental Section

Materials: Hexadecyltrimethylammonium chloride (CTAC, 25% W/W), L-ascorbic acid (≥99%), sodium hypochlorite solution (10–15% available chlorine), sodium borohydride ($NaBH_4$, 99%), poly(ethylene glycol) methyl ether thiol 6000 average molar mass (PEG-6K-SH, M_n = 6000 g mol^{-1}), poly(diallyldimethylammonium chloride) (PDDA, average M_w = 100 000–200 000), poly(acrylic acid sodium salt) (PAA, M_w = 15 000), hydrogen peroxide (H_2O_2, 28%), sulfuric acid (H_2SO_4, 98%), ethanol (EtOH, 99.8%), commercial samples of kynurenine (25 mg), tryptophan (1 g), ATP (1 g), adenosine (1 g), adenine (1 g), hypoxanthine (1 g), inosine (1 g), IFN-ϒ, and staurosporine drug were supplied by Sigma–Aldrich. Hydrogen tetrachloroaurate trihydrate ($HAuCl_4 \cdot 3H_2O$, ≥99.9%) from Alfa Aesar was employed without further purification. Polydimethylsiloxane (Sylgard 184) was bought from Dow Corning. Water purified with a Milli-Q system was used in all experiments

Synthesis of Au Nanoparticles and Fabrication of Plasmonic Substrates—LbL Methodology: Citrate-stabilized Au NP (30 nm in diameter) were synthesized according to a previously reported seeded growth method.[47] The production of randomly deposited AuNP multilayers was based on the well-known LbL assembly methodology. Following this protocol, glass slides were sequentially immersed in polyelectrolyte solutions of PDDA (1 mg mL^{-1}, 0.05 M NaCl), PAA (1 mg mL^{-1}, 0.05 M NaCl), and (PDDA 1 mg mL^{-1}, 0.05 M NaCl) for 15 min. AuNP layers were then formed by immersing the polyelectrolyte-coated glass slides in a 0.9×10^{-3} M AuNP solution for at least 3 h, followed by rising with water and drying under nitrogen flow. For the deposition of the second and third AuNP layers, the same procedure as described above was repeated.

Template-Assisted Self-Assembly: All nanostructured substrates were prepared on glass cover slips (Menzel-Gläser, Nr 1.5) precleaned with a dilute solution of Helmanex III. AuNPs were synthesized and functionalized with PEG-6K-SH (Sigma—Aldrich), by adding 1 mg of PEG-6K-SH per milliliter of 5×10^{-3} M solution of AuNPs, following a previously reported seed-mediated approach.[48] An optimized cleaning procedure was required prior to the SERS measurements. To this end, the nanoparticle assemblies were treated first with oxygen plasma (Diener PICO, 0.4 mbar O_2, 200 W) and then exposed to UV–O_3 treatment. It was observed that these cleaning treatments may alter the final SERS results, so it is crucial to optimize the exposure time and check the absorbance spectra of the substrate before and after cleaning (Figure S22, Supporting Information).

Cell Culture: HeLa cells were cultured using Dulbecco's modified Eagle medium (DMEM) supplemented with 10% fetal calf serum (FCS). Cells were passaged or used for experiments when they reached 80% confluence. HeLa cells were harvested in a 12-well plate at the concentration of 6×10^4 cell mL^{-1}.

Induction of IDO-1 Enzyme Expression in HeLa Cells: In order to control the activation of IDO-1 in HeLa cells, HeLa cells were harvested in the presence or in the absence of IFN-ϒ (100 ng mL^{-1}) for 48 h. This activation process was reported to correlate with the expression of high amounts of IDO protein.[49] As soon as the activation process finished, the cell media were exchanged and defined concentrations of diverse metabolites were added. This cell media contained varying concentrations of Trp depending on the cell experiment, 10×10^{-6} M of hemin, 2% FCS, and 20% of DMEM diluted in hank´s balanced salt solution (HBBS) buffer. After 24 h of cell culture under these conditions, the cell supernatant was collected and measured by SERS.

Q-RT_PCR: With the aim of studying the IDO-1 induction by IFN-ϒ activation, HeLa cells were harvested in the presence or the absence of IFN-ϒ (100 ng mL^{-1}) for 72 h. RNA was extracted using NucleoSpin RNA isolation kit from Macherey-Nagel (Ref: 740 955.240C). 1 µg of total RNA was used for complementary DNA (cDNA) synthesis using qScript cDNA Supermix from Quanta (Ref: 95 048). Quantitative real-time polymerase chain reaction (qRTPCR) was performed as previously described.[50] Universal Probe Library (Roche) primers and probes employed are as follows: For: gtgtttcaccaaatccacga, Rv: ctgatagctgggggttgc; probe: 20. All qRTPCR data presented

were normalized using glyceraldehyde-3-phosphate dehydrogenase (Hs 0 275 8991_g1 from Applied Biosystems).

Stress Condition Cell Assays: Cells were first harvested in a 12-well plate, at the concentration of 6×10^4 cell mL^{-1} and let 24 h for cell attachment. Consecutively, cell media were exchanged to recreate the stress conditions. About 50×10^{-6} M of H_2O_2 or 5×10^{-6} M of staurosporine drug was added to a control cell medium containing 2% FCS and 20% of DMEM diluted in HBBS buffer or to a starvation medium not containing amino acids, such as HBBS buffer. After 24 h of cell culture under these conditions, the cell supernatant was collected, centrifuged (3500 rpm, 5 min) and measured by SERS.

SERS Measurements: Cell supernatant derived from different biological assays was sampled, and 100 µL of the liquid was deposited on a plasmonic substrate surrounded using a hydrophobic pen (Sigma), which prevented from liquid spreading. All biological studies were performed in three independent cell assays, which were spiked on three independent plasmonic substrates. Finally, SERS spectra were recorded under a 785 nm laser line, obtaining bands' characteristic of metabolite vibrations. As a rule, 25 points from different substrate areas were measured every time. For data processing, the background of SERS spectra following a polynomial curve was removed, and the average spectrum of the 25 points for each condition was obtained by using Renishaw's WiRE software. Then, the characteristic bands of the molecules of interest (Trp 760 cm^{-1}, Kyn 560 cm^{-1}, and HX 725 cm^{-1}) were identified and their intensities were acquired. In Figure 2, the ratio between kynurenine and tryptophan (760 cm^{-1}) was calculated as the division between the intensities at Kyn 560 cm^{-1} and Trp 760 cm^{-1}. Mean ± standard deviation (SD) values were calculated from the three independent cell assays. SERS mapping demonstrated the SERS-enhancing ability of the organized discrete AuNP assemblies in the nanostructured substrate (Figure S3, Supporting Information).

Cell Viability Assay: Cells were seeded at a density of 6×10^4 cell mL^{-1} in 12-well plates and let 24 h for cell attachment. Subsequently, cell media were exchanged to recreate stress conditions, varying either hemin or staurosporine concentrations. After 24 h, cells were fixed in formalin (1 mL per well) and washed with PBS. Then, 0.5 mL of 0.1% crystal violet was added, which bound to the cells in 20% methanol. The plate was cleaned with deionized (DI) water and crystal violet interacting with the cells was resuspended in 10% acetic acid. Finally, this volume was transferred to a spectrophotometer cuvette to measure the absorbance at 595 nm, which correlates with the number of live cells.

HPLC: Kynurenine and tryptophan samples' separation was performed in reversed-phase chromatography using an ACQUITY UPLC BEH C18 1.7 µm (2.1 × 100 mm) column (Waters, Manchester, UK), which was maintained at 30 °C. For hypoxanthine and inosine, ACQUITY UPLC BEH Amide 1.7 µm (2.1 × 50 mm) columns were used. The injected sample volume in all cases was 10 µL, and the autosampler was set at 4 °C. For kynurenine and tryptophan, the mobile phase was designed as phase A, consisting of a mixture of 0.1% formic acid–H_2O and phase B, acetonitrile. The method used a gradient at constant flow rate (0.3 mL min^{-1}) combining solvent A and solvent B, programmed as follows: 0–0.5 min, linear change from A–B (95:5 v/v) to A–B (1:99 v/v) in 2.5 min and finally returning to 95% A at 3.7 min for column re-equilibration, which was completed at 5 min. For hypoxanthine and inosine, the same mobile phase was used at 0.5 mL min^{-1} with the following gradient: 0–0.5 min, linear change from A–B (5:95 v/v) to A–B (50:50 v/v) in 2.5 min and finally returning to 5% A at 4.1 min. The peaks were characterized by comparing the retention time and UV–vis absorbance at $\lambda = 363$ nm for kynurenine, $\lambda = 277$ nm for tryptophan and $\lambda = 249$ for hypoxanthine and inosine.

Cancer-On-A-Chip Assays: To print the cancer-on-a-chip device, silicone ink was prepared using an elastomer base (Shin-Etsu Silicone) with a curing agent at a 10:1 volume ratio and the mixture was loaded into a 10 mL clear syringe (PSY-E; Musashi Engineering, Ltd.) and printed with a diameter of 2 cm by a multiheaded 3D Discovery bioprinter (RegenHU, Switzerland) on a glass microslide (26 × 76 mm). HeLa cells were seeded into collagen-based hydrogels, 3 mg mL^{-1} of collagen final concentration, after sequential trypsinization and centrifugation. Consecutively, 80 µL of the mixture formed by cells with collagen solution was laden inside the silicon chamber, and the gel-filled devices were then placed in prepared humid chambers in a CO_2 incubator to allow collagen to polymerize at 37 °C for 20 min. Next, The cell media (2% FCS and 20% of DMEM diluted in HBBS buffer) were added with different staurosporine/hemin concentrations and the samples were incubated for 24 h. The cell device was then assembled with the plasmonic substrate, placing the gold nanoparticle assembly directly in contact with the extracellular milieu. All noncommercial substrates were thoroughly cleaned and exposed to the UV lamp for 20 min, to reduce the risk of biological contamination. Finally, the plasmonic substrate was illuminated with a 785 nm laser to record SERS spectra. For cell viability imaging, cells were incubated with CytoCalcein for 30 min, and the samples were then washed three times with 1×PBS and imaged with a Cell Axio Observer microscope.

Supporting Information

Supporting Information is available from the Wiley Online Library or from the author.

Acknowledgements

J.P. acknowledges an FPU fellowship from the Spanish Ministry of Science, Innovation and Universities. L.M.L.-M. acknowledges funding from the European Research Council (ERC AdG 787510, 4DbioSERS) and the Maria de Maeztu Units of Excellence Program from the Spanish State Research Agency (Grant No. MDM-2017-0720). C.G.-A. acknowledges a Juan de la Cierva Fellowship from the Spanish Ministry of Science, Innovation and Universities (FJCI-2016-28887). The authors thank Dr. J. Calvo and Dr. D. Otaegui at CIC biomaGUNE for support with LC/ESI-HRMS measurements. The work of A.C. was supported by the Basque Department of Industry, Tourism and Trade (Elkartek), and the department of education (IKERTALDE IT1106-16, also participated by A. Gomez-Muñoz), the BBVA foundation, the MINECO (SAF2016-79381-R (FEDER/EU); Severo Ochoa Excellence Program SEV-2016-0644-18-1; Excellence Networks SAF2016-81975-REDT), European Training Networks Project (H2020-MSCA-ITN-308 2016 721532), the AECC (IDEAS175CARR, GCTRA18006CARR), La Caixa Foundation (HR17-00094), and the European Research Council (starting Grant 336343, PoC 754627). CIBERONC was co-funded with FEDER funds and funded by ISCIII. A.M. acknowledges funding from the European Research Council (Consolidator Grant 819242) and the Spanish Ministry of Science, Innovation and Universities for the excellence program SEV-2015-0496.

Conflict of Interest

The authors declare no conflict of interest.

Keywords

3D hydrogels cancer cell models, plasmonic substrates, surface-enhanced Raman scattering, tumor environment, tumor metabolism sensing

Received: December 12, 2019
Revised: February 6, 2020
Published online:

[1] C. A. Lyssiotis, A. C. Kimmelman, *Trends Cell Biol.* **2017**, *27*, 863.
[2] U. E. Martinez-Outschoorn, M. Peiris-Pagés, R. G. Pestell, F. Sotgia, M. P. Lisanti, *Nat. Rev. Clin. Oncol.* **2017**, *14*, 11.
[3] A. Arruabarrena-Aristorena, A. Zabala-Letona, A. Carracedo, *Sci. Adv.* **2018**, *4*, eaar2606.
[4] B. Wegiel, M. Vuerich, S. Daneshmandi, P. Seth, *Front. Oncol.* **2018**, *8*, 284.
[5] H. Wang, F. Franco, P. C. Ho, *Trends Cancer* **2017**, *3*, 583.
[6] P. J. Murray, *Nat. Immunol.* **2016**, *17*, 132.
[7] D. Anastasiou, *Br. J. Cancer* **2017**, *116*, 277.
[8] O. Takikawa, T. Kuroiwa, Yamazaki, R. Kido, *J. Biol. Chem.* **1988**, *263*, 2041.
[9] S. Yong, S. Lau, *J. Chromatogr. A* **1979**, *175*, 343.
[10] A. S. Edison, J. L. Markley, R. Bru, H. R. Eghbalnia, R. Powers, D. Raftery, D. S. Wishart, *Curr. Opin. Biotechnol.* **2017**, *43*, 34.
[11] W. Lu, X. Su, M. S. Klein, I. A. Lewis, O. Fiehn, J. D. Rabinowitz, *Annu. Rev. Biochem.* **2017**, *86*, 277.
[12] V. Ntziachristos, M. A. Pleitez, S. Aime, K. M. Brindle, *Cell Metab.* **2019**, *29*, 518.
[13] J. Langer, D. Jimenez de Aberasturi, J. Aizpurua, R. A. Alvarez-puebla, B. Auguie, J. J. Baumberg, G. C. Bazan, S. E. J. Bell, A. Boisen, A. G. Brolo, J. Choo, D. Cialla-May, V. Deckert, L. Fabris, K. Faulds, F. J. García de Abajo, R. Goodacre, D. Graham, A. J. Haes, C. L. Haynes, C. Huck, S. A. Maier, T. Mayerhöfer, M. Moskovits, K. Murakoshi, J. M. Nam, S. Nie, Y. Ozaki, I. Pastoriza-Santos, J. Perez-Juste, et al. *ACS Nano* **2020**, *14*, 28.
[14] G. Bodelón, V. Montes-García, V. López-Puente, E. H. Hill, C. Hamon, M. N. Sanz-Ortiz, S. Rodal-Cedeira, C. Costas, S. Celiksoy, I. Pérez-Juste, L. Scarabelli, A. La Porta, J. Pérez-Juste, I. Pastoriza-Santos, L. M. Liz-Marzán, *Nat. Mater.* **2016**, *15*, 1203.
[15] N. Feliu, M. Hassan, E. Garcia Rico, D. Cui, W. J. Parak, R. A. Alvarez-Puebla, *Langmuir* **2017**, *38*, 9711.
[16] B. Kang, L. A. Austin, M. A. El-sayed, *ACS Nano* **2014**, *8*, 4883.
[17] D. Lin, J. Pan, H. Huang, G. Chen, S. Qiu, H. Shi, W. Chen, Y. Yu, S. Feng, R Chen, *Sci. Rep.* **2014**, *4*, 4751.
[18] C. Yorucu, K. Lau, S. Mittar, N. H. Green, A. Raza, I. U. Rehman, S. MacNeil, *Appl. Spectrosc. Rev.* **2016**, *51*, 243.
[19] V. Shalabaeva, L. Lovato, R. La Rocca, G. C. Messina, M. Dipalo, E. Miele, M. Perrone, F. Gentile, F. De Angelis, *PLoS One* **2017**, *12*, e0175581.
[20] M. Hassoun, I. W. Schie, T. Tolstik, S. E. Stanca, C. Krafft, J. Popp, *Beilstein J. Nanotechnol.* **2017**, *8*, 1183.
[21] F. Lussier, D. Missirlis, J. P. Spatz, J. F. Masson, *ACS Nano* **2019**, *13*, 1403.
[22] F. Lussier, T. Brulé, M. Vishwakarma, T. Das, J. P. Spatz, J. F. Masson, *Nano Lett.* **2016**, *16*, 3866.
[23] K. Renner, K. Singer, G. E. Koehl, E. K. Geissler, K. Peter, P. J. Siska, M. Kreutz, *Front. Immunol.* **2017**, *8*, 248.
[24] K. Singer, W.-C. Cheng, M. Kreutz, P.-C. Ho, P. J. Siska, *Dis. Models Mech.* **2018**, *11*, dmm034272.
[25] G. Bodelón, V. Montes-García, C. Costas, I. Pérez-Juste, J. Pérez-Juste, I. Pastoriza-Santos, L. M. Liz-Marzán, *ACS Nano* **2017**, *11*, 4631.
[26] C. Hanske, E. H. Hill, D. Vila-Liarte, G. González-Rubio, C. Matricardi, A. Mihi, L. M. Liz-Marzán, *ACS Appl. Mater. Interfaces* **2019**, *11*, 11763.
[27] C. Matricardi, C. Hanske, J. L. Garcia-Pomar, J. Langer, A. Mihi, L. M. Liz-Marzán, *ACS Nano* **2018**, *12*, 8531.
[28] S. Nie, C. G. Castillo, K. L. Bergbauer, J. F. R. Kuck, I. R. Nabiev, N. T. Yu, *Appl. Spectrosc.* **1990**, *44*, 571.
[29] Q. Tu, J. Eisen, C. Chang, *J. Biomed. Opt.* **2010**, *15*, 020512.
[30] S. S. De Ravin, K. A. Zarember, D. Long-Priel, K. C. Chan, S. D. Fox, J. I. Gallin, D. B. Kuhns, H. L. Malech, *Blood* **2010**, *116*, 1755.
[31] J. E. Cheong, L. Sun, *Trends Pharmacol. Sci.* **2018**, *39*, 307.
[32] N. T. Nguyen, A. Kimura, T. Nakahama, I. Chinen, K. Masuda, K. Nohara, Y. Fujii-Kuriyama, T. Kishimoto, *Proc. Natl. Acad. Sci. USA* **2010**, *107*, 19961.
[33] E. Lenzi, D. Jimenez de Aberasturi, L. M. Liz-Marzán, *ACS Sens.* **2019**, *4*, 1126.
[34] W. Däubener, N. Wanagat, K. Pilz, S. Seghrouchni, H. G. Fischer, U. J. Hadding, *J. Immunol. Methods* **1994**, *168*, 39.
[35] M. T. Nelp, P. A. Kates, J. T. Hunt, J. A. Newitt, A. Balog, D. Maley, X. Zhu, L. Abell, A. Allentoff, R. Borzilleri, H. A. Lewis, Z. Linz, S. P. Seitz, C. Yanz, J. T. Groves. *Proc. Natl. Acad. Sci. USA* **2018**, *115*, 3249.
[36] J. Basran, I. Efimov, N. Chauhan, S. J. Thackray, J. L. Krupa, G. Eaton, G. A. Griffith, C. G. Mowat, S. Handa, E. L. Raven, *J. Am. Chem. Soc.* **2011**, *133*, 16251.
[37] W. R. Premasiri, J. C. Lee, A. Sauer-budge, R. Théberge, C. E. Costello, L. D. Ziegler, *Anal. Bioanal. Chem.* **2016**, *408*, 4631.
[38] S. Chiang, S. Chen, L. Chang, *Int. J. Mol. Sci.* **2019**, *20*, 39.
[39] L. Antonioli, C. Blandizzi, P. Pacher, G. Haskó, *Nat. Rev. Cancer* **2013**, *13*, 842.
[40] F. Di Virgilio, E. Adinolfi, *Oncogene* **2017**, *36*, 293.
[41] Y. J. Wang, R. Fletcher, J. Yu, L. Zhang, *Genes Dis.* **2018**, *5*, 194.
[42] C. Hernandez, P. Huebener, R. F. Schwabe, *Oncogene* **2016**, *35*, 5931.
[43] S. W.-Y. Chiu, H.-W. Cheng, Z.-X. Chen, H.-H. Wang, M.-Y. Lai, J.-K. Wang, Y.-L. Wang, *Phys. Chem. Chem. Phys.* **2018**, *20*, 8032.
[44] J. Kabir, M. Lobo, I. Zachary, *Biochem. J.* **2002**, *367*, 145.
[45] H. Yi, Y. H. Jeong, Y. Kim, Y. Choi, H. E. Moon, D. Cho, *Nat. Biomed. Eng.* **2019**, *3*, 509.
[46] J. Yu, E. Berthier, A. Craig, T. E. de Groot, S. Sparks, P. N. Ingram, D. F. Jarrard, W. Huang, D. J. Beebe, A. B. Theberge, *Nat. Biomed. Eng.* **2019**, *3*, 830.
[47] N. G. Bastús, J. Comenge, V. Puntes, *Langmuir* **2011**, *27*, 11098.
[48] C. Hanske, G. González-Rubio, C. Hamon, P. Formentín, E. Modin, A. Chuvilin, A. Guerrero-Martínez, L. F. Marsal, L. M. Liz-Marzán, *J. Phys. Chem. C* **2017**, *121*, 10899.
[49] B. Jürgens, U. Hainz, D. Fuchs, T. Felzmann, A. Heitger, *Blood* **2009**, *114*, 3235.
[50] V. Torrano, L. Valcarcel-Jimenez, A. R. Cortazar, X. Liu, J. Urosevic, M. Castillo-Martin, S. Fernández-Ruiz, G. Morciano, A. Caro-Maldonado, M. Guiu, P. Zuñiga-García, M. Graupera, A. Bellmunt, P. Pandya, M. Lorente, N. Martín-Martín, J. D. Sutherland, P. Sanchez-Mosquera, L. Bozal-Basterra, A. Zabala-Letona, A. Arruabarrena-Aristorena, A. Berenguer, N. Embade, A. Ugalde-Olano, I. Lacasa-Viscasillas, A. Loizaga-Iriarte, M. Unda-Urzaiz, N. Schultz, A. M. Aransay, V. Sabz-Moreno, et al. *Nat. Cell Biol.* **2016**, *18*, 645.